Review Article ISSN 2832-9384

Journal of Materials and Polymer Science

# Fabrication of CuNPs Integrated Reduced Graphene Oxide Nanocomposite for Efficient SERS Material

**Garima Dang, Srikrishna Manna and Samar Kumar Medda***

*CSIR-Central Glass and Ceramic Research Institute, 196, Raja S. C. Mullick Road, Kolkata 700032, India.*

***Corresponding author**

**Samar Kumar Medda,**
CSIR-Central Glass and Ceramic Research Institute, 196, Raja S. C. Mullick Road, Kolkata 700032, India.

Submitted: 7 Oct 2026; **Accepted:** 19 Oct 2026; **Published:** 24 Nov 2026

**Citation:** S. K. Medda et al. (2026). Fabrication of CuNPs Integrated Reduced Graphene Oxide Nanocomposite for Efficient SERS Material. *J mate poly sci, 6*(3) :1-14. DOI : https://doi.org/10.47485/2832-9384.1087

**Abstract**

*Inherent properties of 'wonder material', graphene can be experienced by integrating it with different nanomaterials to form unique composite materials. So, metal-graphene nanocomposites are major focus in research due to its unique and outstanding properties. Graphene is known to exhibit many free electrons which can be used to trap nanoparticles (NPs). In this work, a simple synthetic route was developed to prepare a copper nanoparticles (Cu NPs) - reduced graphene oxide (RGO) composite (Cu/RGO) via a chemical reduction method. Metallic copper is prone to aerial oxidation when exposed to atmosphere. However, Cu NPs get stabilized when embedded in the RGO sheets or matrices, unlike bare Cu. The Cu/RGO nanocomposites prepared with varying Cu to GO weight ratios were characterized by different spectroscopic and microscopic techniques. The average crystallite size of Cu NPs in Cu/RGO (2:5) composite was found to be 14 nm. This Cu/RGO (2:5) nanocomposite was used in surface enhanced Raman scattering (SERS) as a SERS active substrate. The SERS activity of this nanocomposite was studied using methylene blue (MB) as a probe molecule. The MB was detected at an ultralow concentration of $10^{-8}$ M with an enhancement factor of $10^{7}$, implying its ultrahigh sensitivity can serve as a very efficient SERS substrate. This novel approach could be used for various applications such as sensing of bioanalytes and photocatalytic activities, food safety & analysis, catalyst and environmental monitoring as well as highly valuable in marine areas particularly, useful for marine antifouling and corrosion protection coatings and wastewater purification.*

**Keywords:** GO, Cu/RGO nanocomposite, SERS, methylene blue (MB), Raman spectra.

## Introduction

Graphene, usually described as "wonder material" of the 21st century, has changed the dimensions of nanoscience and nanotechnology. Graphene is a single layer of pure carbon foundation of graphitic materials built in all dimensions; it can be wrapped up into 0D fullerenes, rolled into 1D nanotube or stacked into 3D graphite (Geim & Novoselov, 2007). Graphene exhibits many unique properties in terms of electrical and thermal conductivity, optical, mechanical, high carrier mobility at room temperature etc (Shaker et al., 2025; Zarbali et al., 2012; Zhu et al., 2024; Tiwari et al., 2020; Lu et al., 2026). Various synthetic routes have been developed to modify the properties for various applications. Graphene and its derivatives (graphene oxide (GO) and reduced graphene oxide (RGO)) are prepared via many synthetic routes ranging from the bottom-up epitaxial growth (Magro et al., 2025; Maroulas et al., 2025; He et al., 2023; Saputra et al., 2025) to the top-down exfoliation of graphite can be prepared through chemical routes like oxidation, intercalation and sonication (Li et al., 2008; Nicolaescu et al., 2024; Ismail et al., 2022; Lotya et al., 2009). In this regard, Hummer's and Offeman explored an alternative method for the oxidation of graphite by adding a mixture of ($KMnO_4$) and concentrated sulphuric acid ($H_2SO_4$) (Hummers & Offeman, 1958). RGO was first reported by using hydrazine hydrate when dispersed in an aqueous medium. After that various methods have been explored for the synthesis of RGO including chemical reduction, thermal mediated reduction and electrochemical reduction but, sodium borohydride ($NaBH_4$) was demonstrated to function more effectively than hydrazine as a reductant of graphene oxide (Dreyer et al., 2010).

## Literature Review

### Graphene based Nanocomposites

Graphene exhibits many unique properties which have led to wide scale research in the synthesis of graphene-based nanocomposites. Graphene based nanocomposites have been successfully synthesized in different combination for various uses using inorganic nanostructures (Muszynski et al., 2008; Zhu et al., 2011; Gedi et al., 2016), organic crystals (Wang et al., 2010; Han et al., 2010), polymers (Wang et al., 2010; Yang et al., 2010), metal–organic frameworks (MOFs) (Jahan et al., 2010; Petit et al., 2011), biomaterials (Lu et al., 2009; Chang et al., 2010), and carbon nanotubes (CNTs) (Dong et al., 2011; Tung et al., 2009), organic dyes (Choudhury et al., 2026; Vo et

al., 2024) and are intensively explored in applications such as batteries (Zhu et al., 2011; Wang et al., 2010), supercapacitors (Zhang et al., 2009), fuel cells (Zhang et al., 2010), photovoltaic devices (Li et al., 2010), photocatalysis (Goktas & Goktas, 2026; Sahin 2025; Goktas et al., 2025; Sahin et al., 2024; Song et al., 2011; Du et al.,2010; Zhang et al., 2010) and so on.

## Metal-Graphene Composites and SERS activities

After Ruoff's group reported on the fabrication of metal-graphene composites, many researchers were encouraged to develop new graphene-based composites. Noble metals such as Au (Goncalves et al., 2009; Choi & Yu, 2012), Ag (Kichukova et al., 2022; Bai et al., 2011), Pt (Bai et al., 2011; Yoo et al., 2009) and Pd (Scheuermann et al., 2009; Li et al., 2010) have been integrated with graphene to synthesize graphene/metal nanocomposites. Apart from this, other metal nanomaterials such as Cu (Bai et al., 2011; Mahadev et al., 2025; Wang et al., 2009), Sn (Bai et al., 2011; Warner et al., 2010), Co (Warner et al., 2010), bimetals (Bian et al., 2011) and alloys (Bai et al., 2011) were also used to fabricate the inorganic composites of graphene. These metal-graphene nanocomposites are used for applications such as photo-catalytic activity and surface enhanced Raman Scattering (SERS). SERS is a powerful and non-destructive technique for the detection of probe molecules adsorbed on the surface of metal nanoparticles. Various kinds of SERS active substrates have been studied such as colloidal nanoparticles, metal islands, electrochemically roughened electrodes etc. T. T. H. Pham et al. reported Ag/ZnO metal-semiconductor hybrid as SERS substrate derived via reduction using $NaBH_4$ with SERS performance EF for $10^{-4}$ M of MB reached $6.2 \times 10^6$ (Pham et al., 2022). Recently, Quan-Doan Mai et al. reported $Fe_3O_4$@C@$TiO_2$ semiconductor nanostructures as a SERS substrate capable of activating and amplifying the Raman signal of MB with maximum EF of $5.4 \times 10^5$ (Mai et al., 2016). To date Au and Ag nanoparticles with graphene materials have been extensively studied due to their extraordinary plasmon resonance properties and its application as active SERS substrate with SERS value in the range of ($10^8$ to $10^9$) have been reported (Hao et al., 2012; Santos et al., 2025).

## Mechanism of SERS enhancement

SERS is defined as the amplification of Raman scattered signals through the molecules adsorbed on irregular surfaces of metal nanoparticles. This powerful analytical technique can detect molecular species at extremely low concentrations. There was a breakthrough in the field of spectroscopy ever since the first observation of enhanced signals of pyridine adsorbed on roughened metallic electrode surface of silver in 1970's. (Fleischmann et al., 1974). However, the enhanced spectra were not recognized by the authors at that time. It was in 1977, SERS was later properly interpreted by Van Duyne and Albrecht, and Albrecht and Creighton. They reported SERS, a novel phenomenon showing outstanding enhancement in Raman signals due to probe molecules adsorbed on the irregular surfaces of metallic particles (Haynes et al., 2005). The electric field enhancement was proposed by Jeanmaire and Van Duyne whereas the Albrecht and Creighton speculated the concept of molecular interaction of probe molecule to the metal surface and electronic states (Albrecht & Creighton, 1977). Since then, tremendous amount of research interest has been directed towards SERS.

The two mechanisms which are responsible for the enhancement of inelastic light scattering are electromagnetic and chemical enhancement. Electromagnetic Enhancement – A major part of enhancement is contributed to electromagnetic enhancement, due to the excitation of the localized surface plasmon resonances resulting in the amplification of the light intensity (Santos et al., 2025). Interaction of light with the irregular surfaces of the metal leads to excitation of conduction electron (Surface Plasmon Resonance). Localized surface Plasmon resonance (LSPR) is the excitation of electron wave which can increase both elastic (Rayleigh) and inelastic scattering. The theoretical calculation of the electromagnetic enhancement is up to ~ $10^{10}$-$10^{11}$.

Chemical Enhancement – It occurs because of a charge transfer effect or chemical bond formation between metal surfaces and probe molecules. The enhancement factor due to chemical enhancement is upto ~ $10^2$-$10^3$ (Santos et al., 2025).

## Cu/RGO Nanocomposite

Copper metal is easily available with low cost as compared to Au, Ag, Pt etc metals. In this regards the prohibitive cost and poor scalability as well as weaker chemical mechanism (CM) and charge-transfer synergies of Au/Ag in the hybrid graphene system are limited when compared to Cu. Moreover, plasmonic property of copper is also good which can be used in applications such as photocatalytic, electrocatalytic and SERS activity. However, the major drawback of metallic copper is that it is unstable. When exposed to airy atmosphere metallic copper oxidizes to a dominant product of a major $Cu_2O$ and minor CuO. To stabilize copper many protective techniques have been used such as chemical vapour deposition, microemulsion, chemical reduction in aqueous solution, sono-chemical reduction, laser ablation, thermal reduction, electrochemical methods and hydrothermal process. One such method is reduction of metallic Cu using RGO as a supporting matrix. The synthesis of Cu-RGO nanocomposites are widely reported for different applications such as fabrication of CuNPs/ GO composites for SERS using GO and $CuCl_2$ (Zhang, 2012), synthesis of CuO/RGO using GO and $CuCl_2$ through one step redox reaction for electrocatalytic activity towards catenol oxidation organic pollutant (Zhao et al., 2012), one-Pot synthesis of CuS/rGO nanocomposite using GO and $CuCl_2$, $H_2SO_4$ towards enhanced photocatalytic performance (Zhang et al., 2012), synthesis of CuNPs on RGO as a highly active and recyclable catalyst for synthesis of formamides and primary amines using GO and $CuSO_4.5H_2O$ by ex-situ synthesis (Fakhri et al., 2014), dispersion of CuNPs/RGO using GO and $CuSO_4$ .$5H_2O$ by in situ electro-polymerization using an ionic surfactant as the supporting electrolyte towards electrochemical and electrocatalytic activity (Ehsani et al., 2014). Q. Hao et al. (2012) reported RERS on graphene based metallic nanostructure substrates (Hao et al., 2012) and

Camden reported single molecule SERS (Camden, 2008). Recently G. F. S. dos Santos et al. have described Au, Ag and Cu etc nanoparticle of various morphologies and sizes as SERS material and have been widely explored due to their plasmonic properties, as well as hybrid or combined nanoparticle systems in presence of graphene-based materials (Santos et al., 2025). In this regards, Pal Choudhury et al. (2026) reported CuO-RGO based SERS materials for detection of R6G with $10^{-8}$ M (Choudhury et al., 2026). In general, little attention has been given on Cu and its composite as SERS substrates as well as it's stability with temperature and in different atmospheric conditions.

In this work, we have synthesized Cu/RGO nanocomposite using a simple chemical reduction route. The surface of RGO contains many free electrons capable of trapping Cu nanoparticles which readily gets oxidized in airy atmosphere. Thus, RGO is used as a supporting matrix to stabilize Cu nanoparticles and prevent further oxidation of Cu. The added advantage of RGO is that it also acts a fluorescence quencher. Metallic CuNPs exhibit excellent plasmonic properties and have a higher scope in applications such as sensing of bioanalytes and photocatalytic activities as well as food safety & analysis, catalyst monitoring activities and SERS enhancement as well as highly valuable in marine areas particularly, useful for marine antifouling and corrosion protection coatings and waste water purification (Santos et al., 2025). Here we studied the SERS activity of Cu/RGO nanocomposite using MB as probe molecule. So, the specific aim of this work is to synthesize metal-graphene nanocomposites using copper as a metal. In this work, we attempted to synthesis of Cu/RGO nanocomposites in different weight ratios of Cu to GO using chemical reduction method to study the SERS activity and enhancement factor (EF) of Cu/RGO nanocomposite using MB as a probe molecule for different MB concentrations. The synthesis process is discussed as a function of processing and reducing steps along with stability of Cu/RGO composite in various temperature and different atmospheric conditions. The characteristics of the GO and Cu/RGO composites were evaluated using FTIR and Raman studies, XRD, TEM analysis along with investigation of SERS activities of the composites and compared with the available reported data.

## Materials and Methods Materials

The chemicals used for this work are as follows. Graphite powder (particle size < 20 μm) and sodium nitrate ($NaNO_3$) were purchased from Sigma Aldrich, Potassium permanganate ($KMnO_4$), Sulphuric acid ($H_2SO_4$) hydrochloric acid (HCl; 35.4%), hydrogen peroxide ($H_2O_2$; 30%), copper (II) chloride ($CuCl_2$) were obtained from Merck, sodium borohydride ($NaBH_4$) was obtained from SRL Pvt. Ltd. Ammonia solution ($NH_4OH$) was purchased from RANKEM (RFCL Pvt. Ltd.). Millipore water (18 MΩ) obtained from Milli-Q system was used as a solvent. All the reagents were used as received.

## Synthesis of Graphene Oxide (GO)

Graphene Oxide was prepared using the well-known modified Hummer's method (Hammers & Offeman, 1958). 1 gm of graphite powder and 0.5 gm of $NaNO_3$ were mixed with 70 ml of $H_2SO_4$ in a triple neck round bottom flask (Figure 1) and kept in ice bath (0-5°C) with continuous stirring. The temperature was kept below 20°C, since the reaction of sulfuric acid with $KMnO_4$ is explosive 3 gm of $KMnO_4$ was slowly added to the mixture under stirring condition. The mixture was left for stirring for 2 h. After 2 h, 100 ml of water was added slowly to dilute the solution. The reaction temperature slightly increased with effervescence and color of the mixture changed to dark brown. Water was added slowly while maintaining the flask temperature below 20°C in an ice bath, as an uncontrolled temperature increase could cause a runaway reaction. After that 5 wt. % $H_2O_2$ was added dropwise until the color of the solution changes to bright yellow which indicated that graphene oxide (GO) was completely oxidized (Haynes et al., 2005). The graphite slurry thus obtained was washed with 1N HCl and $H_2O$ successively to remove the excess sodium and potassium ions and collected by centrifuge at the speed of 5000 rpm for 10 minutes. The final product was obtained after being dried in oven at 60°C for 16 h.

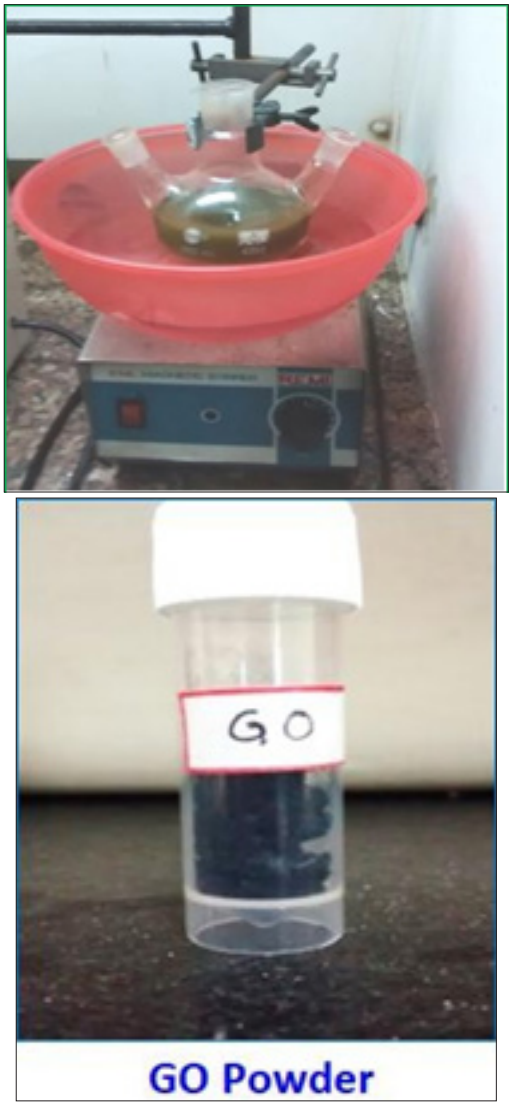


**Figure 1:** The photographs represent the experimental setup for the preparation of graphene oxide (GO) from graphite powder by the modified Hummer's method, and the prepared GO.

### Synthesis of Cu/RGO nanocomposite

75 mg of GO prepared by the above-mentioned method was ultrasonically dispersed in water. 30 mg of copper (II) chloride and 65 mg of sodium borohydride were mixed with 12.5 and 5 ml of water separately in two other flasks. The molar ratio of $CuCl_2$ to $NaBH_4$ was maintained at 1:10. The $CuCl_2$ and GO ratio were kept at 2:5. Then the three mixtures were mixed and stirred for 15 minutes at room temperature. 2-3 drops of dil. NH3 was added to the mixture after 15 minutes. The mixture was kept under stirring for 1 h. After 1 h, the mixture was filtered using a 0.22 µm polyvinylidene fluoride (PVDF) membrane and washed several times with distilled water. The resultant mixture was then dried in oven at 60°C for 3-4 h and obtained composite is shown in figure 2 and detailed synthesis procedure is given in figure 1S (see in the supporting information). This sample was labeled as Cu-RGO (2:5) or Cu/RGO (2:5). Similar way other Cu-RGO nanocomposites were also synthesized by varying Cu and GO weight ratios whose details and sample labeling are given in table 1.



**Figure 2:** Photograph of the prepared Cu/RGO nanocomposite (in an alumina ceramic crucible boat) after drying at 60°C for 3-4 h.

**Table 1:** Synthesis of Cu-RGO nanocomposites with varying Cu to GO weight ratios using $NaBH_4$ as a reducing agent.

| Cu-RGO Nanocomposite | GO (mg) | $CuCl_2$ (mg) | $NaBH_4$ (mg) |
|---|---|---|---|
| Cu-RGO (1:5) | 75 | 15 | 32.5 |
| Cu-RGO (2:5) | 75 | 30 | 65 |
| Cu-RGO (4:5) | 75 | 60 | 130 |
| Cu-RGO (8:5) | 75 | 120 | 260 |

### Sample Preparation for SERS Experiment

To study SERS the Raman activity methylene blue (MB) was chosen as a probe molecule. Choice of MB was made because of its low fluorescence quantum yield (0.02±0.005). 5 wt% of the sample and MB solutions of different molar concentrations ($10^{-4}$, $10^{-6}$ and $10^{-8}$) order, respectively were ultrasonically dispersed. The mixture was dispersed for about 10 minutes and out of this mixture 10 µL was dropped cast on aluminium (Al) substrate (sheet) for collecting Raman spectra.

### Characterization

GIXRD of the samples were measured with a Rigaku SmartLab X-ray diffractometer operating at 9 kW (200 mA, 45 kV) using Cu Kα (λ = 1.5406 Å) radiation. The Raman spectra of the samples were recorded at room temperature (25±2°C) on Renishaw in Via Reflex micro-Raman spectrometer (Class 3B, serial no-02H669), using A 785 nm diode laser as the excitation source. 20x objective lens was used with sport diameter of ~1 µm. Infrared absorption spectra of the film deposited on both side polished Si-wafers were recorded by FTIR spectrometry (Nicolet, 380) with a resolution of 4 $cm^{-1}$ and 200 scans. Transmission electron microscopic (TEM) measurements were carried out with a JEOL 2010 transmission electron microscope equipped with an EDS (energy dispersive X-ray scattering) facility.

TEM samples were prepared by dispersion of Cu/RGO in water and then placed on Mo grid. Inductively Coupled Plasma Mass Spectrometer (ICP-MS), Perkin-Elmer, USA was used for mass analysis. For this analysis, 10 gm of powdered sample (Cu/RGO) was taken in a crucible and heat treated at 300°C in reducing atmosphere ($H_2$). After reduction the resultant mixture was weighed again (0.67 gm) and aqua regia (a mixture of nitric acid and hydrochloric acid in molar ratio of 1:3) was added to it. The sample was allowed to absorb in the aqua regia and evaporated to dryness. This procedure was repeated three times, and the final sample was absorbed in 1% of $HNO_3$ making the volume up to 250 ml. The sample constituents were then measured using ICP-MS.

## Results and Discussion

### Properties of the GO and Cu/RGO nanocomposites

The entire synthesis process of Cu nanoparticle (Cu NPs) modified reduced graphene oxide (Cu/RGO) is schematically presented in figure 3. The Cu NPs incorporated or embedded RGO was synthesized by chemical reduction method using $NaBH_4$ as reducing agent and $NH_4OH$ as pH adjuster. At first the ultrasonication was used to synthesize fine particles of GO which form a stable dispersion in water. Then $CuCl_2$ was dissolved in the colloidal dispersion of GO in water. The mixed solution was stirred for 30 min to allow the significant interaction between $CuCl_2$ and GO. Then the $NaBH_4$ was added to the solution followed by addition of $NH_4OH$ to maintain the pH of the solution at around 12. During the chemical reduction process $CuCl_2$ was reduced to form Cu nanoparticles (Cu NPs). When the pH was maintained at ~12 by using $NH_4OH$, the $Cu^{2+}$ was transformed to $Cu(OH)_2$. The resultant $Cu(OH)_2$ was then reduced by $NaBH_4$ and produced Cu NPs (Quing-Ming et al., 2012). Moreover, during this reduction process the elimination of oxygen-containing functional groups such as hydroxyl, epoxy, carboxylic acid, carbonyl and peroxides groups on GO sheets occur using $NaBH_4$ as reducing agent to form RGO.

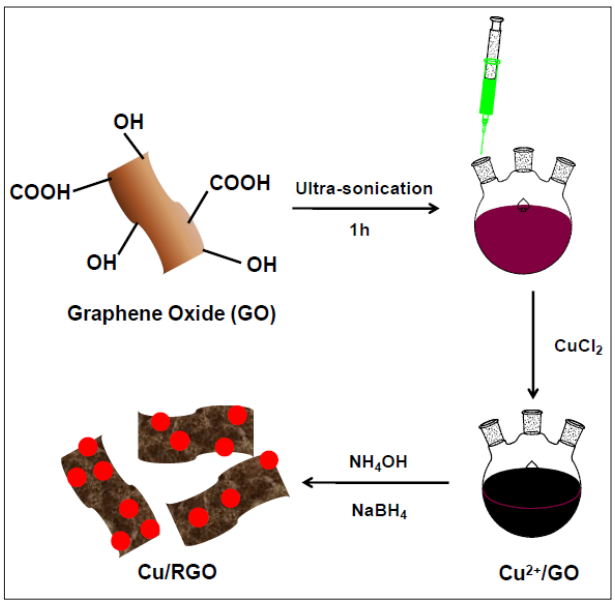


**Figure 3:** Schematic representation of the formation of Cu nanoparticles (Cu NPs) modified reduced graphene oxide (Cu/RGO) composite via $NaBH_4$ reduction.

## XRD Analysis

The Cu/RGO nanocomposites were characterized by XRD. As shown in figure. 4. GO has a characteristic 2θ peak at 10.2 corresponding to its interlayer distance $d_{002}$=0.75 nm. Figure 4 shows the phase and crystallinity of Cu/RGO synthesized in three different ratios. The sharp and intense peaks of 2θ values at 43.4°, 50.5° and 74.3° can be indexed to (111), (200) and (220) planes of face-centred cubic lattice of metallic Cu. The small peak at 36.25° (111) depicts the presence of trace amount of cuprous oxide. The crystallite sizes of Cu were determined by using X-ray line broadening method from the high intensity peaks (111), and the crystallite size was found to be ~14 nm. The crystallite size (measured using Scherrer formula) of Cu/RGO (4:5) and Cu/RGO (8:5) composites was found to be 12 nm and 13 nm, respectively (Goktas et al., 2015; Goktas, 2018). XRD also confirmed the presence of RGO in the composites. A broad peak at 25.48° clearly indicates that GO was successfully reduced to RGO. XRD patterns of GO and Cu-RGO (2:5) as prepared along with different temperature and atmospheric conditions were also studied (Figures 2S; supporting information) for stability and to check the formation of copper oxide. Further, from Raman analysis (Figure 3S and Figure 4S; supporting information) it shows that this copper oxide transformation is prominent for temperatures above 300 °C but at lower temperature oxide formation is absent due to presence of graphene-hybrid system, the graphene matrix protects Cu from oxidation (Santos et al., 2025). However, this oxide formation is also almost absent in reducing atmosphere ($H_2$) even at temperature >300 °C.

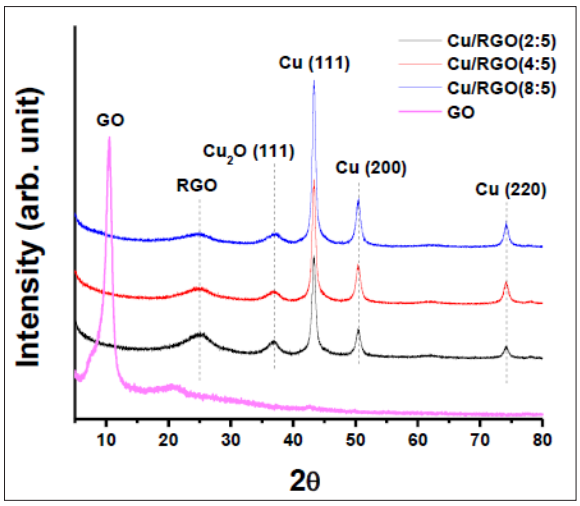


**Figure 4:** XRD patterns of synthesized GO and Cu/RGO nanocomposites prepared with varying weight ratios of Cu to GO using $NaBH_4$ as reducing agent.

## FTIR Analysis

FT-IR spectrum of the graphene oxide obtained in these steps confirms the successful oxidation of the graphite as shown in figure 5. The presence of different type of oxygen functionalities in graphene oxide (GO) was confirmed at 3400 $cm^{-1}$ (O-H stretching vibrations), at 1720 $cm^{-1}$ (stretching vibrations from COOH), at 1600 $cm^{-1}$ (skeletal vibrations from unoxidized graphitic domains), at 1220 $cm^{-1}$ (epoxy stretching vibrations), and at 1060 $cm^{-1}$ (C-O stretching vibrations) (Xu et al., 2008). In Cu/RGO (2:5) composite FTIR peaks related to O-H stretching vibrations observed at 3400 $cm^{-1}$ as well as epoxy (C-O) and other C-O peaks intensity were also significantly reduced due to deoxygenation or reduction. However, stretching vibrations from C=O at 1650 $cm^{-1}$ and C—O stretching vibrations at 1060 $cm^{-1}$ were still observed due to remaining oxygenated groups at edges even after chemical reduction (Li et al., 2008). This also implies that the effective elimination of oxygen-containing functional groups—such as hydroxyl, epoxy, carboxylic acid, carbonyl and peroxides groups on the surface and basal planes of the GO sheets using $NaBH_4$ as reducing agent to form RGO.

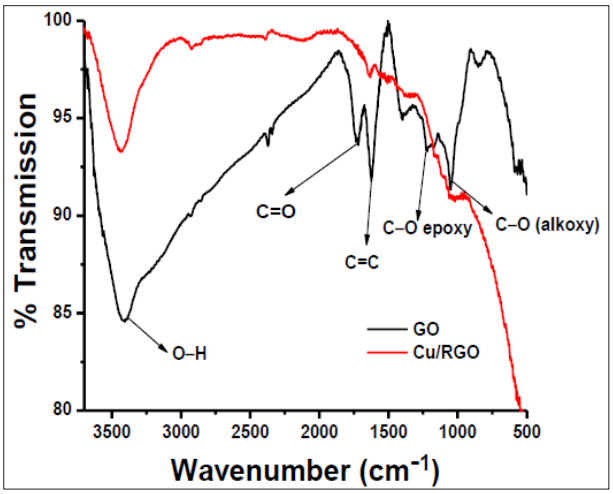


**Figure 5:** The FTIR spectra of GO and Cu/RGO (2:5) composite show deoxygenation of oxygen containing functional groups on GO sheets to form RGO after reduction.

## Raman Analysis

The GO and Cu/RGO nanocomposite were successfully characterized by Raman spectroscopy (Figure. 6). It can be noted that GO has lots of functional groups attached to its basal plane causing a significantly less graphitic nature and more $sp^3$ character. For this reason, GO showed only D and G bands, and no distinguishable 2D band in its Raman spectrum (Figure 6). The characteristic G band at 1595 $cm^{-1}$, implies the vibration of $sp^2$ hybridized carbon which corresponds to the doubly degenerate zone center E2g mode of graphite and D band at 1354 $cm^{-1}$ implies, the defect band due to misaligned hexagonal graphitic layers (Ferrari & Robertson, 2000; Garf et al., 2007). The *ID/IG* ratio 0.84 where ID and IG are the intensities of D and G band corresponds to the defect density of the graphene-based materials. The Raman spectra of Cu/RGO with peak at about 1307 $cm^{-1}$ (D band) and at 1590 $cm^{-1}$ (G band) is clearly observed from figure 6. The ID/IG ratio of Cu/RGO is 2.1 which is slightly higher than that of GO. The increased ID/IG ratio clearly indicates that due to reduction, large number of new graphitic domains of smaller dimensions were created in Cu/RGO. Detailed systematic studies of Raman Spectra of GO and Cu-RGO (2:5) nanocomposite at different temperature and atmospheric conditions are also shown in figure 3S and figure 4S (see in the supporting information). From this analysis it shows that copper oxide formation of Cu/RGO composite is almost absent, especially at lower temperature as well as in reducing atmosphere ($H_2$) even at >300 °C temperature.

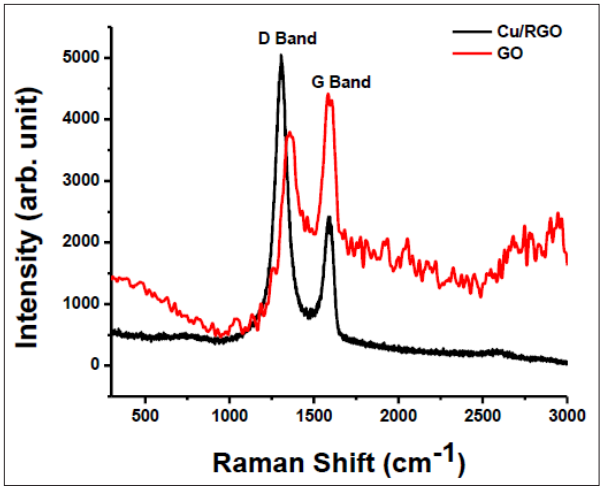


**Figure 6:** Raman spectra of GO and Cu/RGO (2:5) nanocomposite with D and G band.

## ICP-MS Analysis

The ICP-MS analysis gives the amount of total Cu present in the composites. From this analysis we observed that about 23% Cu was present in the Cu/RGO (2:5) composites.

## TEM study

TEM study was performed to characterize the composites material. TEM (by STEM technique) images with different magnifications (Figures 7 a, b) and the EDX pattern of the Cu/RGO (2:5) composites are shown in figure 7c. Presence of Cu NPs and Cu/RGO can be seen in the TEM images. The average crystallite size of Cu nanoparticle in the Cu/RGO (2:5) composite was found to be 14 nm. EDX analysis (Figure 7 c) also clearly shows the existence of Cu and C (originated from RGO) in the composite. The lattice spacing shown in the HR-TEM image (inset in Fig. 7b) is close to 0.20 nm, which agrees with the (111) lattice spacing of Cu, indicating these small nanoparticles are Cu crystals. Diffraction peaks in the SAED pattern also confirm the signature of Cu NPs (inset in Fig. 7a).

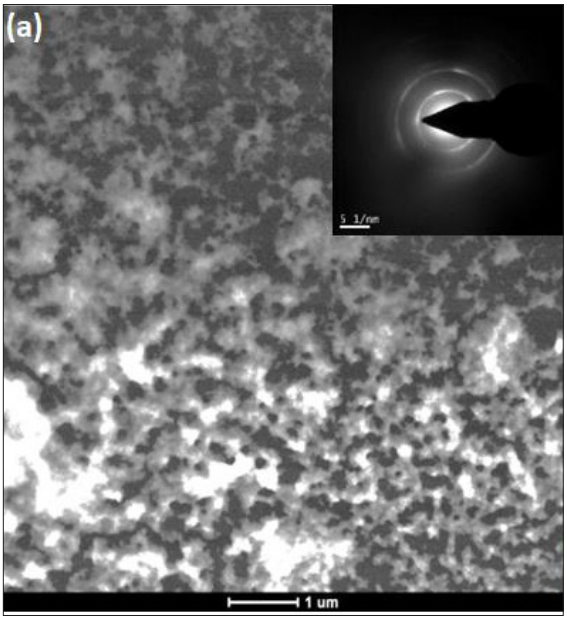


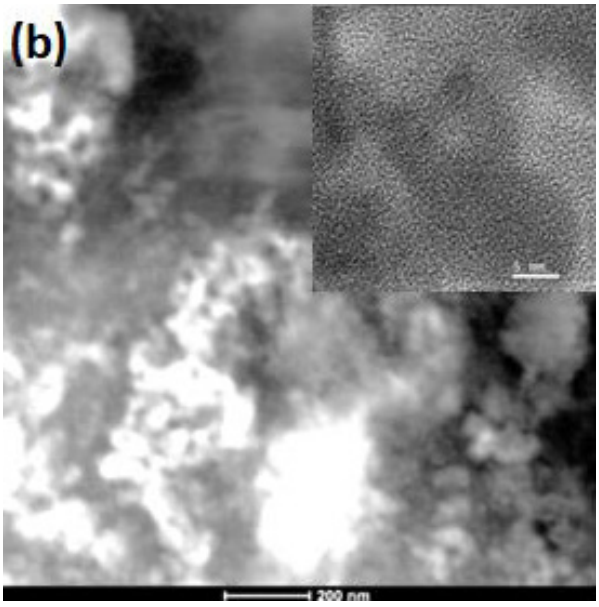

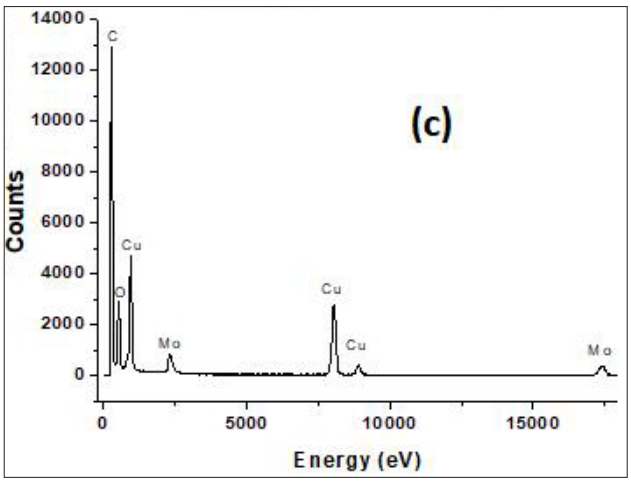


**Figure 7:** TEM (by STEM technique) images with different magnifications (Figure a, b) along with EDX pattern (Figure c) of the Cu/RGO (2:5) composites. The insets in Figures a and b display the SAED and HR-TEM patterns, respectively. Mo grid has been used for TEM study due to sample contains Cu.

### SERS properties of the Cu/RGO composites

The Cu/RGO nanocomposite was employed as a potential substrate material for SERS application. Methylene blue was chosen as a probe molecule to measure the SERS activity of Cu/RGO nanocomposite. MB is an aromatic dye which strongly absorbs around wavelength 670 nm with low fluorescence quantum yield (0.02±0.005) (Atherton & Harriman, 1993). To investigate the SERS activity Cu/RGO was ultrasonically dispersed in MB solutions of varying concentrations ($10^{-4}$, $10^{-6}$ and $10^{-8}$) and from that solution 10 µL was dropped cast on Al sheet. The Raman spectra of the samples were collected using a diode laser of 785 nm. The laser power was adjusted at 1%, with a laser spot of 1 µm focused using 20x objective.

The laser was exposed in an area of 1 µm for 15 seconds and spectra were taken 5-6 times for each case to check the reproducibility of the SERS substrate. All the measurements were taken in the line focus mode, and the laser power was kept sufficiently low to avoid any damage of the SERS active substrate.

As the main absorption peaks of the MB located at around 656, 610 and 693 are away from the excitation wavelength (785 nm), the resonant Raman effect would be very weak (Xiao & Man, 2007; Camargo et al., 2010). The characteristic Raman band of MB absorbed on Cu/RGO nanocomposite at 445 $cm^{-1}$ and 1618 $cm^{-1}$ due to C-C stretching and C-N-C skeletal bending of MB, respectively can be clearly observed, which indicates that the skeletal bending was well adsorbed on the substrates (Naujok et al., 1993).

In this work we have examined the performance of SERS activity of bare Cu NPs using MB solution of concentration $10^{-4}$ M (Figure 8). Due to the SERS activity of in presence and absence of bare Cu NPs, we observed that there was a small enhancement in the Raman peak at 1618 $cm^{-1}$. But the intensity of the Raman peak at 1618 $cm^{-1}$ was found more than two times in presence of Cu/RGO composites as compared to bare Cu NPs under similar condition. This phenomenon can be explained considering charge transfer (CT) from RGO to MB which results in the enhancement of SERS signal intensity basically known as chemical enhancement (Ling et al., 2010). Fluorescence background interferes with the Raman signal which causes a huge problem to obtain the signature of a fluorescent molecule like MB by resonance Raman spectroscopy as shown in figure 9. RGO acts as a fluorescence quencher and thus becomes an effective SERS substrate for MB (Xie et al., 2009). The maximum SERS enhancement was found in Cu/RGO (2:5) nanocomposite (Figure 9). Further increase in Cu loading it was observed that the Raman enhancement was decreased. We may conclude that as the Cu loading was increased, the effect of RGO surface decreased, thereby decreasing slightly the enhancement activity. However, the particle sizes of the Cu NPs embedded

Cu/RGO nanocomposites prepared at different weight ratios was almost same (~14 nm). Hence, it is confirmed that the RGO matrix plays an important role for SERS enhancement. In this regard SERS enhancement in Cu/RGO (1:5) composite was found to be low compared to other ratios, so, this system was not discussed.

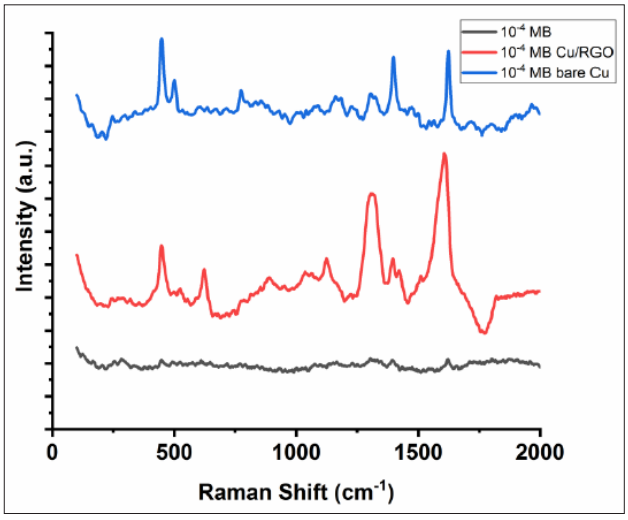


**Figure 8:** Raman enhancement spectra of MB solution of $10^{-4}$ M concentration in presence and absence of Cu nanoparticles along with Cu/RGO composite.

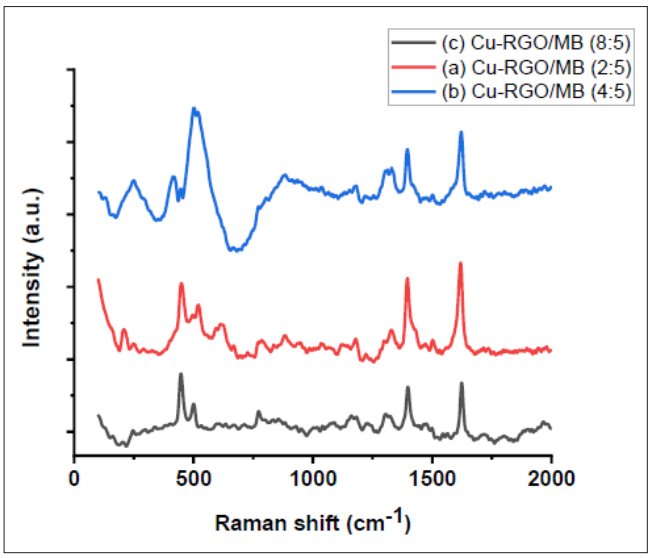


**Figure 9:** SERS spectra of Cu-RGO/MB with varying different Cu/RGO nanocomposite (a) Cu-RGO (2:5) (b) Cu-RGO (4:5) and (c) Cu-RGO (8:5). For this study MB solution of $10^{-4}$ M concentration was used.

It has been reported that graphene has become a new class of SERS substrate for efficient Raman scattering of a molecule adsorbed on graphene surface. From the figure 9, it is clearly observed that the SERS enhancement value of Cu/RGO (2:5) composite is maximum as compared to other ratios. So, details SERS experiment for Cu-RGO (2:5) was performed using varying concentrations of MB solution ($10^{-4}$, $10^{-6}$, and $10^{-8}$ M) (Figure 10). The spectra of MB with molar concentrations ($10^{-4}$, $10^{-6}$, and $10^{-8}$ M) exhibit strong intensities due to SERS effect. The enhancement factor per molecule of Cu/RGO can be estimated using the following expressions (Felidj et al., 2002; Hunyadi & Murphy, 2006):

$$EF = (I_{Sers} \times N_{Bulk}) / (I_{Raman} \times N_{Abs})$$

Where $I_{Sers}$ is the intensity of the surface enhanced spectrum and $I_{Raman}$ is the intensity of normal Raman spectrum. $N_{Bulk}$ is the number of MB molecules present in the laser spot and $N_{Abs}$ is the number of probe molecules adsorbed on the SERS active substrate. In our calculations, the enhancement factor was evaluated taking 1618 $cm^{-1}$ Raman shift into consideration. The enhancement factors of different concentrations ($10^{-4}$, $10^{-6}$, and $10^{-8}$ M order) of MB dispersed with Cu/RGO (2:5) were calculated as: 1.28 x $10^{8}$, 3.25 x $10^{7}$ and 1.9 x $10^{7}$, respectively. The SERS improvement with ultrahigh sensitivity of the Cu/RGO (2:5) composite may probably of electromagnetic enhancement of SERS signal due to proximity of the Cu NPs on the RGO surface in combination with chemical interaction between 'S+' in MB dye and Cu NPs embedded RGO can also lead to additional enhancement effects (Choudhury et al., 2026). The detailed calculation of enhancement factor has been given in the supporting information. The SERS spectra of MB solution of different concentrations are given in figure 10. It is observed that as the concentration of the analyte (MB) decreases the enhancement factor also decreases. Notably, the high SERS sensitivity and enhancement factor of the Cu/RGO (2:5) nanocomposite synthesized in this work were found be comparable to the reported values (mostly in the order of to ) for Au-or Ag-graphene hybrid systems (Hao et al., 2012 & Santos et al., 2025) and can serve as other applications (Li et al., 2021; Xu et al., 2022; Xu et al., 2018).

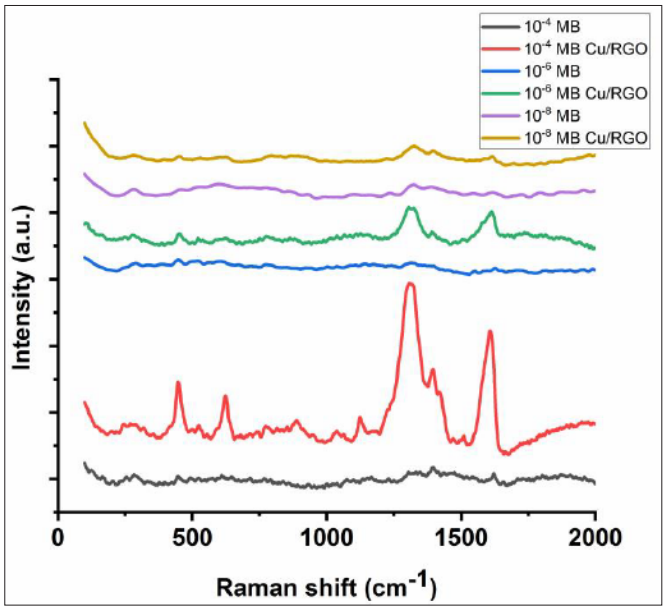


**Figure 10:** SERS spectra of Cu/RGO (2:5) nanocomposite obtained using MB solution of concentrations: (a) $10^{-4}$ M, (b) $10^{-6}$ M and (c) $10^{-8}$ M.

## Conclusions

Based on the work we can conclude that the synthesis of Cu/RGO nanocomposite was successfully accomplished via a simple chemical reduction method. Cu/RGO nanocomposites were characterized by Raman, FTIR, XRD, ICP-MS and TEM analysis. SERS experiments were carried out in a systematic way, the results obtained from composites showed successful SERS detection of MB molecules of varying concentrations ($10^{-4}$ to$10^{-8}$ M). The embedment of Cu nanoparticles on RGO sheets via reduction method improves the stability of Cu NPs which are, in general prone to quick oxidation into copper oxide. The SERS enhancement factors using $10^{-4}$, $10^{-6}$ and $10^{-8}$ M concentrations of MB dispersed with Cu/RGO (2:5) were calculated to be 1.28 x $10^{8}$, 3.25 x $10^{7}$ and 1.9 x $10^{7}$, respectively. It was also observed that the Cu/RGO composite can even sense up to $10^{-10}$ M concentration of MB. Considering cost-effectiveness with relatively stable alternatives to gold, silver, Pt materials and comparable ultrahigh sensitivity making Cu/RGO composite material as very efficient SERS substrate with strong potential for various uses. This novel approach could be used for applications such as sensing of bioanalytes and photocatalytic activities, forensics as well as food safety & analysis, environmental and catalyst monitoring.

## Associated Content

### Supporting Information

The Supporting Information is available free of charge at at https://unisciencepub.com/ journal-of-materials-and-polymer-science/

Schematic representation of preparation of GO and RGO, XRD spectra of (a) GO, (b) Cu-RGO as prepared, (c) Cu-RGO heated at 350 °C air and (d) Cu-RGO heated at 350 °C reduced at 300 °C under an H2 atmosphere, Raman Spectra of Cu-RGO nanocomposite at different temperature, Raman Spectra of Cu-RGO nanocomposite at different temperature and atmospheric conditions.

## Conflicts of Interest

The authors declare that they have no conflicts of interest.

## Author Contributions

Dr. Samar Kumar Medda: Investigation, conceptualization, methodology, visualization, writing – original draft and funding acquisition, Garima Dang: Investigation, experiment and writing, Dr. Srikrishna Manna: writing – review & editing, visualization.


## Acknowledgements

The Authors thank to the Director, CSIR-CGCRI for encouraging this work. Financial support funded by CSIR, Govt. of India (CGCRI/BDPD/ Project - OM-22-23/35; dated 01/02/2023) is appreciatively acknowledged.


## References


1. Geim, A. K., & Novoselov, K. S. (2007). The Rise of Graphene. Nat. Mater, 6, 183–91. DOI: https://doi.org/10.1038/nmat1849
2. Shaker, L. M., Abdulamier, A. A. & Al-Amiery, A. A. (2025). Graphene-based materials for next-generation energy storage: Progress, challenges, and future outlook. *J. Alloys Compd.*, 1036, 182079. DOI: https://doi.org/10.1016/j.jallcom.2025.182079
3. Zarbali, M., Göktaş, A., Mutlu, I., Kazan, S., Şale, A. G. & Mikailzade, F. (2012). Structure and Magnetic Properties of La0.66Sr0.33MnO3Thin Films Derived Using Sol-Gel Technique. *J. supercond. Nov. Magn., 25*(8), 2767-2770. DOI: https://doi.org/10.1007/s10948-011-1260-z
4. Zhu, P. J., Yan, Y. N., Zhou, Y., Qi, Z. J., Li ,Y. F. & Chen, C. M. (2024). Thermal Properties of Graphene and Graphene-Based Nanocomposites: A Review. ACS Appl. *Nano Mater., 7*(8), 8445–8463. DOI: https://doi.org/10.1021/acsanm.4c00411
5. Tiwari, S. K., Sahoo, S., Wang, N. & Huczko, A. (2020). Graphene research and their outputs: Status and prospect. *J. Sci.: Adv. Mater. Devices, 5*(1), 10-29. DOI: https://doi.org/10.1016/j.jsamd.2020.01.006
6. Lu, Z., Ding, G., Mei, Q., Zheng, B., Chen, K., Wang, H., Han, X. & Shao, J. (2026). Graphene-Doped Ammonium Oxalate-Derived Carbon Aerogel with Controllable Structure for Synergistic Endothermic-Insulating Efficient Thermal Protection. *Gels, 12*(6), 535. DOI: https://doi.org/10.3390/gels12060535
7. Magro, M. R., Vella, D. A. & Cassar, G. (2025). Synthesis of graphene oxide: A refined approach. *Carbon Trends*, 20, 100509-100518. DOI: https://doi.org/10.1016/j.cartre.2025.100509
8. Maroulas, K. M., Vordos, N., Mitropoulosa, A. C. & Kyzas, G. Z. (2025). Nanobubbles in graphene oxide synthesis: investigation of structure and physicochemical properties with boosting of oxygen content and microporous surface area. *RSC Adv., 15*(21), 16525–1653. DOI: https://doi.org/10.1039/d5ra02336j
9. He, T., Xiong, S., Han, H., Wang, D., Wang, Y., Dai, C. & Liu, W. (2023). Facile synthesis of Ag/GO SERS composite with highly sensitive and stable performance. Colloids Surf. A Physicochem. Eng. Asp., 662, 131008. DOI: https://doi.org/10.1016/j.colsurfa.2023.131008
10. A. A.,Saputra, A. A., Marpongahtun, Andriayani, R. Goei, R., Tok, A. I. Y., Goutianos, S. & Gea, S. (2025). "Facile synthesis of reduced graphene oxide using natural plant extracts as green reducing agents", *J. King Saud Univ. Eng. Sci., 37*(5), 16. DOI: https://doi.org/10.1007/s44444-025-00007-9
11. Li, D., Muller, M. B., Gilje, S., Kaner, R. B. & Wallace, G. G. (2008). Processable aqueous dispersion of graphene nanosheets. Nat. *Nanotechnol.*, 3, 101–105. DOI: https://doi.org/10.1038/nnano.2007.451
12. Nicolaescu, M., Ambrus, S., Hididis, P. Morariu, M., Hulka., I. Orha, C., Lazau, C., Codrean, C., & and Bandas, C. (2024). In Situ Synthesis of NPC-Cu2O/CuO/rGO composite via dealloying and microwave-assisted hydrothermal technique. *Crystals, 14*(11), 968-84. DOI: https://doi.org/10.3390/cryst14110968
13. Ismail, N. A., Shameli, K., Sukri, Siti Nur A. M., Hara, H., Teow, S-Y. & Moeini, H. (2022). Sonochemical synthesis of a copper reduced graphene oxide nanocomposite using honey and evaluation of its antibacterial and cytotoxic activities. *Mol. Biosci.*,9, 995853. DOI: https://doi.org/10.3389/fmolb.2022.995853
14. Lotya, M., Hernandez, Y., King, P. J., Smith, R. J., Nicolosi, V., Karlsson, L. S., Blighe, F. M., De, S., Wang, Z., McGovern, I. T., Duesberg. G. S. & Coleman, J. N. (2009). Liquid phase production of graphene by exfoliation of graphite in surfactant/water. *J. Am. Chem. Soc., 131*(10), 3611–3620. DOI: https://doi.org/10.1021/ja807449u
15. Hummers, W. S. & Offeman, R. E. (1958). Preparation of Graphitic Oxide. *J. Am. Chem. Soc., 80*(6), 1339–1339. DOI: https://doi.org/10.1021/ja01539a017
16. Dreyer, D. R., Park, S., C. W. Bielawski C. W. & Ruoff, R. S. (2010). The chemistry of graphene oxide. *Chem Soc Rev., 39*(10), 228-240. DOI: https://doi.org/10.1039/b917103g
17. Muszynski, R., Seger, B. & Kamat, P. V. (2008). Decorating Graphene Sheets with Gold Nanoparticles. *J. Phys. Chem. C, 112*(14), 5263–5266. DOI: https://doi.org/10.1021/jp800977b
18. Zhu, J., Zhu, T., Zhou, X., Zhang, Y., Lou, X. W., Chen, X., Chen, H., Zhang, H., Hng, H. H., & Yan, Q. (2011). Facile synthesis of metal oxide/reduced graphene oxide hybrids with high lithium storage capacity and stable cyclability. *Nanoscale, 3*(3), 1084–1089. DOI: https://doi.org/10.1039/c0nr00744g

19. Gedi, S., Reddy, V. R. M. Kotte, T. R. R., Kim, S. H. & Jeon, C. W. (2016). Chemically synthesized Ag-doped SnS films for PV applications. Ceram. *Int., 42*(16), 19027-19035. DOI: https://doi.org/10.1016/j.ceramint.2016.09.059
20. Wang, S., Goh, B. M., Manga, K. K., Bao, Q., Yang, P. & Loh, K. P. (2010). Graphene as Atomic Template and Structural Scaffold in the Synthesis of Graphene-Organic Hybrid Wire with Photovoltaic Properties. *ACS Nano, 4*(10), 6180–6186. DOI: https://doi.org/10.1021/nn101800n
21. Han, T. H., Lee, W. J., Lee, D. H., Kim, J. E., Choi, E. Y. & Kim, S. O. (2010). Peptide/Graphene Hybrid Assembly into Core/Shell Nanowires. *Adv. Mater., 22*(18), 2060–2064. DOI: https://doi.org/10.1002/adma.200903221
22. Yang, H. F., Zhang, Q. X., Shan, C. S., Li, F. H., Han, D. X. & Niu, L. (2010). Stable, Conductive Supramolecular Composite of Graphene of Graphene Sheets with Conjugated Polyelectrolyte. *Langmuir, 26*(9), 6708–6712. DOI: https://doi.org/10.1021/la100365z
23. Jahan, M., Bao, Q., Yang, J. X. & Loh, K. P. (2010). Structure-Directing Role of Graphene in the Synthesis of Metal-Organic Framework nanowire. *J. Am. Chem. Soc., 132*(41), 14487–14495. DOI: https://doi.org/10.1021/ja105089w
24. Petit, C., Burress, J. & Bandosz, T. J. (2011). The synthesis and characterization of copper-based metal-organic framework/graphite oxide composites. *Carbon, 49*(2), 563–572. DOI: https://doi.org/10.1016/j.carbon.2010.09.059
25. Lu, C. H., Yang, H. H., Zhu, C. L., Chen, X. & Chen, G. N. (2009). A graphene platform for sensing biomolecules. Angew. *Chem., Int. Ed., 48*(26), 4785-7. DOI: https://doi.org/10.1002/anie.200901479
26. Chang, H., Tang, L., Wang, Y., Jiang, J. & Li, J. (2010). Graphene fluorescence resonance energy transfer aptasensor for thrombin detection. *Anal. Chem., 82*(6), 2341–2346. DOI: https://doi.org/10.1021/ac9025384
27. Dong, X., Li, B., Wei, A., Cao, X., Chan-Park, M. B., Zhang, H., Li, L. J., Huang, W. & Chen, P. (2011). One-step growth of graphene-carbon nanotube hybrid materials by chemical vapour deposition. *Carbon, 49*(9), 2944–2949. DOI: https://doi.org/10.1016/j.carbon.2011.03.009
28. Tung, V. C., Chen, L. M., Allen, M. J., Wassei, J. K., Nelson, K., Kaner, R. B. & Yang, Y. (2009). Low-temperature solution processing of graphene-carbon nanotube hybrid materials for high-performnace transparent conductors. *Nano Lett., 9*(5), 1949–1955. DOI: https://doi.org/10.1021/nl9001525
29. Choudhury, B. P., Dagar, T., Halder, D., Sarkar, R., Sarkar, S., Mondal, S., Pramanick, S., Chowdhury, J., Jana, Y. & De, S. (2026). Cost-effective production of copper oxide nanoparticle-doped rGO materials under mild conditions-recyclable photocatalytic degradation of toxic dyes and SERS sensing at ultralow concentrations. Mater. *Chem. Phys*., 350, 131920-131933. DOI: https://doi.org/10.1016/j.matchemphys.2025.131920
30. Vo, T. M., Nguyen, T. My H. & Wung Bark, C. (2024). Reduced Graphene Oxide-Supported Copper(I) Oxide Composites for the Degradation of Methylene Blue: Exploring the Capacity of RGO as an Electron Capturer for Achieving Highly Stable Photocatalytic Activity. ACS Appl. Electron. *Mater., 6*(6) 4391-4405. DOI: https://doi.org/10.1021/acsaelm.4c00479
31. Zhu, J., Zhu, T., Zhou, X., Zhang, Y., Lou, X. W., Chen, X, Chen, H., Zhang, H. Hng, H. H., & Yan, Q, (2011). Facile Synthesis of metal oxide/reduced graphene oxide hybrids with high lithium storage capacity and stable cyclability. *Nanoscale, 3*(3), 1084–1089. DOI: https://doi.org/10.1039/c0nr00744g
32. Wang, H., Cui, L.F., Yang, Y., Sanchez Casalongue, H., Robinson, J. T., Liang, Y. Cui, Y. & Dai, H. (2010). Mn3O4-Graphene Hybrid as a High-Capacity Anode Material for Lithium Ion Batteries. *J. Am. Chem. Soc., 132*(40), 13978–13980. DOI: https://doi.org/10.1021/ja105296a
33. Zhang, Y., Li, H., Pan, L., Lu, T, & Sun, Z. (2009). Capacitive behavior of graphene-ZnO composite film for supercapacitors. *J. Electroanal. Chem., 634*(1), 68-71. DOI: https://doi.org/10.1016/j.jelechem.2009.07.010
34. Zhang, L.S., Liang, X.Q., Song, W.G. & Wu, Z.Y. (2010). Identification of nitrogen species on N-doped graphene layers and Pt/NG composite catalyst for direct methanol fuel cell. *Phys. Chem. Chem. Phys., 12*(38), 12055–12059. DOI: https://doi.org/10.1039/c0cp00789g
35. Li, X., Zhu, H., Wang, K., Cao, A., Wei, J., Li, C., Jia, Y., Li, Z., Li, X. & Wu, D. (2010). Graphene-On-Silicon Schottky Junction Solar Cells. *Adv. Mater., 22*(25), 2743–2748. DOI: https://doi.org/10.1002/adma.200904383
36. Göktaş, A. & Göktaş, S. (2026). Effect of Ti concentration on the defect-engineered photocatalytic and ferromagnetic properties of Co-doped ZnO thin films. Surf. *Interfaces,* 94, 109622-47. DOI: https://doi.org/10.1016/j.surfin.2026.109622
37. Şahin, G. (2025). Tuning photocatalytic activity of La0.67K0.33MnO3 perovskite thin films: Critical role of annealing temperature. Ceram. *Int., 51*(25 (Part C)), 47218-47230. DOI: https://doi.org/10.1016/j.ceramint.2025.07.425
38. Goktas, A., Yesilçimen, M., Kilic, A., Goktas, S. & Tumbul, A. (2025). Synergistic Co–Cu dual doping in ZnS thin Films: Unlocking high room-temperature ferromagnetism and UV-activated photocatalytic efficiency for multifunctional applications. *Mater. Chem. Phys*., 346, 131399-131409. DOI: https://doi.org/10.1016/j.matchemphys.2025.131399
39. Sahin, G., Goktas, A. & Aslan, E. (2024). A new way to tune photocatalytic activity, surface morphology, and structural/optical parameters of ZrO2 thin films using different Zr sources along with annealing temperature and film thickness. *J. Sol-Gel Sci. Technol*., 112 (2), 425-443. DOI: https://doi.org/10.1007/s10971-024-06534-2?urlappend=%3Futm_source%3Dresearchgate.net%26utm_medium%3Darticle
40. Song, J., Yin, Z., Yang, Z., Amaladass, P., Wu, S., Ye, J., Zhao, Y., Deng, W., Zhang, H. & Liu, X. (2011). Enhancement of photogenerated electron transport in dye-synthesized solar cells with introduction of a reduced graphene oxide-TiO2 junction. *Chem. Eur. J., 17*(39),

10832 – 10837.
DOI: https://doi.org/10.1002/chem.201101263
41. Du, J. Lai, X., Yang, N., Zhai, J., Kisailus, D., Su, F., Wang, D. & Jiang, L. (2010). Hierarchically Ordered Macro-Mesoporous TiO2-Graphene Composite Films: Improved Mass Transfer, Reduced Charge Recombination and Their Enhanced Photocatalytic Activities. *ACS Nano, 5*(1), 590–596. DOI: https://doi.org/10.1021/nn102767d
42. Zhang, H., Lv, V., Li, Y. M., Wang, Y. & Li, J. H. (2010). P25-graphene composite as a high performance photocatalyst. *ACS Nano, 4*(1), 380–386.
DOI: https://doi.org/10.1021/nn901221k
43. Goncalves, G., Marques, P. A. A. P., Granadeiro, C. M., Nogueira, H. I. S., Singh, M. K. & Gracio, J. (2009). Surface Modification of Graphene Nanosheets with Gold Nanoparticles: The Role of Oxygen Moieties at Graphene Surface on Gold Nucleation and Growth. *Chem. Mater., 21*(20), 4796–4802.
DOI: https://doi.org/10.1021/cm901052s
44. Choi, K, & Yu, C. (2012). Highly Doped Carbon Nanotubes with Gold Nanoparticles and Their Influence on Electrical Conductivity and Thermo Power of Nanocomposites. *PLoS One, 7*(9), e44977.
DOI: https://doi.org/10.1371/journal.pone.0044977
45. Kichukova, D., Spassova, I., Kostadinova, A., Staneva, A. & Kovacheva, D. (2022). Facile synthesized Cu–RGO and Ag–RGO nanocomposites with potential biomedical applications. *Nanomaterials, 12*(12), 2096-2111.
DOI: https://doi.org/10.3390/nano12122096
46. Bai, S., Shen, X. P., Zhu, G. X., Xu, Z. & Liu, Y. J. (2011). Reversible phase transfer of graphene oxide and its use in the synthesis of graphene-based hybrid materials. *Carbon, 49*(13), 4563–4570.
DOI: https://doi.org/10.1016/j.carbon.2011.06.072
47. Yoo, E., Okata, T., Akita, T., Kohyama, M., Nakamura, J. & Honma, I. (2009). Enhanced electrocatalytic activity of Pt subnanoclusters on graphene nanosheet surface. *Nano Lett., 9*(6), 2255–2259.
DOI: https://doi.org/10.1021/nl900397t
48. Scheuermann, G. M., Rumi, L., Steurer, P., Bannwarth, W. & Muelhaupt, R. (2009). Palladium Nanoparticles on Graphite Oxide and Its Functionalized Graphene Derivatives as Highly Active Catalysts for the Suzuki-Miyaura coupling Rection. *J. Am. Chem. Soc., 131*(23), 8262–8270. DOI: https://doi.org/10.1021/ja901105a
49. Li, N., Wang, Z. Y., Zhao, K. K., Shi, Z. J., Xu, S. K. & Gu, Z. N. (2010). Graphene-PdComposite as Highly Active Catalyst for the Suzuki-Miyaura Coupling Reaction. *J. Nanosci. Nanotechnol., 10*(10), 6748–6751.
DOI: https://doi.org/10.1166/jnn.2010.2638
50. Mahadev, A. P., Kavitha, C., Rose Perutil, J. & John, N. S. (2025). Synergistic SERS enhancement of highly sensitive and reusable rGO-Ag-ZrO2 thin film nanocomposite to detect synthetic textile dyes. *Langmuir, 41*(4), 2411−2426.
DOI: https://doi.org/10.1021/acs.langmuir.4c04105
51. Wang, G. X., Wang, B., Wang, X. L., Park, J., Dou, S. X., Ahn, H. & Kim, K. (2009). Sn/graphene nanocomposite with 3D architecture for enhanced reversible lithium storage in lithium-ion batteries. *J. Mater. Chem., 19*(44), 8378–8384. DOI: https://doi.org/10.1039/b914650d
52. Warner, J. H., Ruemmeli, M. H. Bachmatiuk, A., Wilson, M. & Buechner, B. (2010). Examining Co-Based Nanocrystals on Graphene Using Low-Voltage Aberration-Corrected Transmission Electron Microscopy. *ACS Nano, 4*(1), 470–476.
DOI: https://doi.org/10.1021/nn901371k
53. Bian, J., Wei, X. W. Wang, L. & Guan, Z. P. (2011). Graphene nanosheet as support of catalytically active metal particles in DMC synthesis. Chinese Chemical Letters, 22(1), 57-60.
DOI: https://doi.org/10.1016/j.cclet.2010.07.028
54. Pham, T. T. H., Vu, X. H., Dien, N. D., Trang, T. T., Chi, T. T. K., Phuong, P. H. & Nghia, N. T. (2022). Ag nanoparticles on ZnO nanoplates as a hybrid SERS-active substrate for trace detection of methylene blue *Open Access. RSC Adv., 12*(13), 7850–7863. DOI: https://doi.org/10.1039/D2RA00620K?urlappend=%3Futm_source%3Dresearchgate.net%26utm_medium%3Darticle
55. Mai, Q. D., Trang, D. T. H., Loan, N. T., Hoang, O. V., Bach, T. N., Hoa, N. Q., Tran, N. H. T., Pham, A. T. & Le, A. T. (2026). Charge-transfer-activated SERS detection of methylene blue using an ultrastable, reliable, and highly sensitive semiconductor Fe3O4@C@TiO2 nano-platform Open Access. *RSC Adv., 16*(23), 21152–21167.
DOI: https://doi.org/10.1039/d6ra00307a
56. Hao, Q., Wang, B., Bossard, J. A., Kiraly, B., Zeng, Y. Chiang, I. K., Jensen, L., Werner, D. H. & Huang, T. J. (2012). Surface-Enhanced Raman Scattering Study on Graphene-Coated Metallic Nanostructure Substrates. *J. Phys. Chem. C., 116*(13), 7249−7254.
DOI: https://doi.org/10.1021/jp209821g
57. Santos, G. F. S. dos, Paganoto, G. T., Cosme, L. C., Prado, A. R., Cassini, S. T. A., Guimaraes, M. C. C. & de Oliveira, J. P. (2025). Surface-enhanced Raman spectroscopy as a tool for food and environmental monitoring of pesticides: recent trends and perspectives. *Nanoscale Adv., 7*(22), 7061–7085. DOI: https://doi.org/10.1039/d5na00539f
58. M. Fleischmann, M., Hendra, P. J. & McQuillan, A. J. (1974). Raman spectra of pyridine adsorbed at a silver electrode. *Chem. Phys. Lett., 26*(2), 163-166.
DOI: https://doi.org/10.1016/0009-2614(74)85388-1
59. Haynes, C. L., Mcfarland, A. D. & Van Duyne, R. P. (2005). Surface Enhanced Raman Spectroscopy. *Anal. Chem., 77*(17), 338 A–346 A.
DOI: https://doi.org/10.1021/ac053456d
60. Albrecht, M. G. & Creighton, A. J. (1977). Anamalously Intense Raman Spectra of Pyridine at a Silver Electrode. *J. Am. Chem. Soc., 99*(15), 5215-5217.
DOI: https://doi.org/10.1021/ja00457a071
61. Zhang, K. (2012). Fabrication of copper nanoparticles/graphene oxide composites for surface-enhanced Raman scattering. *Appl. Sur. Sci., 258*(19), 7327-7329.
DOI: https://doi.org/10.1016/j.apsusc.2012.04.002
62. Zhao, Y., Song, X., Song, Q. & Yin, Z. (2012). A facile route to the synthesis copper oxide/reduced graphene oxide nanocomposites and electrochemical detection of catechol organic pollutant. *Crys. Engg. Comm., 14*(20), 6710-6719. DOI: https://doi.org/10.1039/C2CE25509J

63. Zhang, Y., Tian, J., Li, H., Wang, L., Qin, X., Asiri, A. M., Al-Youbi, A. O. & Sun, X. (2012). Biomolecule-Assisted, Environmentally Friendly, One-Pot Synthesis of CuS/Reduced Graphene Oxide Nanocomposites with Enhanced Photocatalytic Performance. *Langmuir, 28*(35), 12893–12900. DOI: https://doi.org/10.1021/la303049w
64. Fakhri, P., Jaleh, B. & Nasrollahzadeh, M. (2014). Synthesis and Characterization of copper nanoparticles supported on reduced graphenemoxide as a highly active and recyclable catalyst for the synthesis of formamides and primary amines. *J. Mol. Catal.A: Chem*, 383-384, 17. DOI: https://doi.org/10.1016/j.molcata.2013.10.027
65. Ehsani, A., Jaleh, B. & M. Nasrollahzadeh, M. (2014). Electrochemical properties and electrocatalytic activity of conducting polymer/copper nanoparticles supported on reduced graphene oxide composite. *J. Power. Sources.*, 257, 300-307. DOI: https://doi.org/10.1016/j.jpowsour.2014.02.010
66. Camden, J. P., Dieringer, J. A., Wang, Y., Masiello, D. J., Marks, L. D., Schatz, G. C., & Van Duyne, R. P. (2008). Probing the structure of single-molecule surface-enhanced Raman scattering hot spots. *J. Am. Chem. Soc., 130*(38), 12616. DOI: https://doi.org/10.1021/ja8051427
67. Quing-ming, L., De-bi, Z., Yamamoto, Y., Kuruda, K. & Okido, M. (2012). Effects of reacton parameters on preparation of Cu nanoparticles via aqueous solution reduction method with NaBH4. Trans. *Nonferrous Met. Soc. China, 22*(12), 2991-2996. DOI: https://doi.org/10.1016/S1003-6326(11)61561-6
68. Goktas, A., Aslan, F. & Tumbul, A. (2015). Nanostructured Cu-doped ZnS polycrystalline thin films produced by a wet chemical route: the influences of Cu doping and film thickness on the structural, optical and electrical properties. *J. Sol-Gel Sci. Technol., 75* (1), 45-53. DOI: https://doi.org/10.1007/s10971-015-3674-8
69. Goktas, A. (2018). High-quality solution-based Co and Cu co-doped ZnO nanocrystalline thin films: Comparison of the effects of air and argon annealing environments. *J. Alloys Compd*., 735, 2038-2045. DOI: https://doi.org/10.1016/j.jallcom.2017.11.391
70. Xu, Y., Bai, H., Lu, G., Li, C. & Shi, G. (2008). Flexible Graphene Films via the Filtration of Water Soluble Noncovalent Functionalized Graphene Sheets. *J. Am. Chem. Soc., 130*(18), 5856–5857. DOI: https://doi.org/10.1021/ja800745y
71. Li, D., Muller, M., Gilje, S., Kaner, R. B. & Wallace, G. G. (2008). Processable aqueous dispersions of graphene nanosheets. *Nature Nanotechnology, 3*(2), 101-105. DOI: https://doi.org/10.1038/nnano.2007.451
72. Ferrari, A. C. & Robertson, J. (2000). Interpretation of Raman spectra of disordered and amorphous carbon. *Phys. Rev. B: Condens. Matter*, 61, 14095. DOI: https://doi.org/10.1103/PhysRevB.61.14095
73. Garf, D., Molitor, F., Esnnlin, K., Stampfer, C., Jungen, A., Hierold, C. & Wirtz, L. (2007). Spatially resolved Raman spectroscopy of single and few-layer graphene. *Nano Lett, 7*(2), 238-242. DOI: https://doi.org/10.1021/nl061702a
74. Atherton, S. J. & Harriman, A. J. (1993). Photochemistry of intercalated methylene blue: photoinduced hydrogen atom abstraction from guanine and adenine. *Am. Chem. Soc., 115*(5), 1816-1822. DOI: https://doi.org/10.1021/ja00058a028
75. Xiao, G. N. & Man, S. Q. (2007). Surface-enhanced Raman scattering of methylene blue adsorbed on cap-shaped silver nanoparticles. *Chem. Phys. Lett., 447*(4-6), 305−309. DOI: https://doi.org/10.1016/j.cplett.2007.09.045
76. Camargo, P. H. C., Au, L., Rycenga, M., Li, W. & Xia, Y. (2010). Meassuring the SERS enhancement factors of dimers with different structures constructed from silver nanocubes. Chem. *Phys. Lett., 484*(4-6), 304−308. DOI: https://doi.org/10.1016/j.cplett.2009.12.002
77. Naujok, R. R., Duevel, R. V. & Corn, R. M. (1993). Fluorescence and Fourier transform surface-enhanced Raman scattering measurements of methylene blue adsorbed onto a sulfur-modified gold electrode. *Langmuir, 9*(7), 1771−1774. DOI: https://doi.org/10.1021/la00031a026
78. Ling, X., Xie, L. M., Fang, Y., Xu, H., Zhang, H. L, Kong, J., Dresselhaus, M. S., Zhang, J. & Liu, Z. F. (2010). Can graphene be used as a substrate for Raman Enhancement?. *Nano Lett., 10*(2), 553-561. DOI: https://doi.org/10.1021/nl903414x
79. Xie, L., Ling, X., Fang, Y., Zhang, J. & Liu, Z. (2009). Graphene as a substrate to suppress fluorescence in Resonance Raman Spectroscopy. *J. Am. Chem. Soc., 131*(29), 9890-9891. DOI: https://doi.org/10.1021/ja9037593
80. Felidj, N., Aubard, J. Levi, G., Krenn, J. R., Salernon, M., Schider, G., Lamprecht, B., Leitner, A. & Aussenegg, F. R. (2003). Optimized surface-enhanced Raman scattering on gold nanoparticle arrays. *Appl. Phys. Lett., 82*(12), 3095–3097. DOI: https://doi.org/10.1063/1.1571979
81. Hunyadi, S. E. & Murphy, C. J. (2006). Bimetallic silver-gold nanowires: fabrication and use in surface-enhanced Raman scattering. *J. Mater. Chem., 16*(40), 3929-3935. DOI: https://doi.org/10.1039/b607116c
82. Li, C., Wu, C., Zhang, K., Chen, M., Wang, Y., Shi, J. & Tang, Z. (2021). The charge transfer effect on SERS in a gold-decorated surface defect anatase nanosheet/methylene blue (MB) system. *New J. Chem., 45*(42), 19775–19786. DOI: https://doi.org/10.1039/d1nj03941e
83. Xu, H., Ma, Y., Chen, J., Zhang, W. X. & Yang, J. (2022). Electrocatalytic reduction of nitrate - a step towards a sustainable nitrogen cycle. *Chem. Soc. Rev., 51*(7), 2710-2758. DOI: https://doi.org/10.1039/d1cs00857a
84. Xu, D., Li, Y., Yin, L., Ji, Y., Niu, J. & Yu, Y. (2018). Electrochemical removal of nitrate in industrial wastewater. *Frontiers of Environmental Science & Engineering (FESE), 12*(1). 9. DOI: https://doi.org/10.1007/s11783-018-1033-z

**Supporting Information**

Fabrication of CuNPs Integrated Reduced Graphene Oxide Nanocomposite for Efficient SERS Material

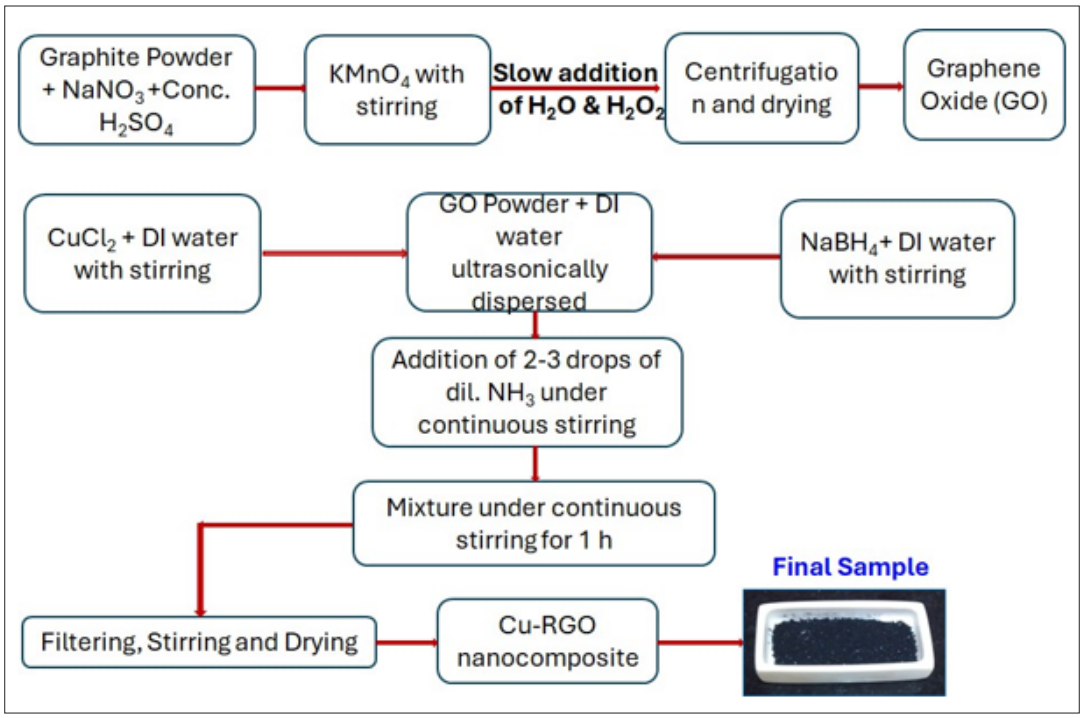


**Figure 1S:** Schematic representation of the preparation of GO and Cu/RGO composites via a wet chemical route.

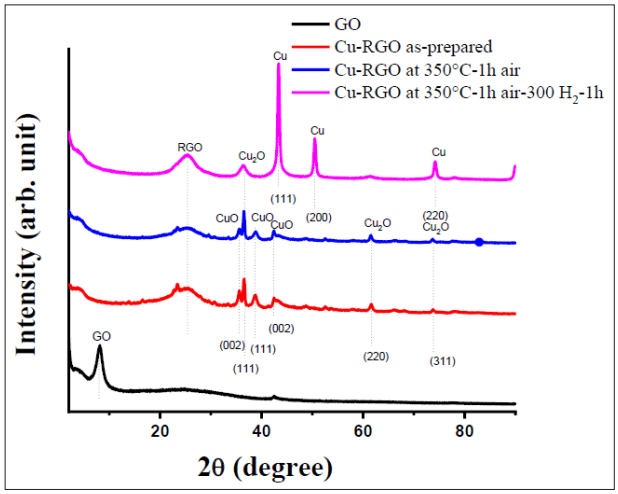


**Figure 2S:** XRD patterns of (a) GO, (b) Cu-RGO as prepared, (c) Cu-RGO heated at 350 °C in air, and (d) Cu-RGO heated at 350 °C in air and subsequently reduced at 300 °C under an $H_2$ atmosphere.

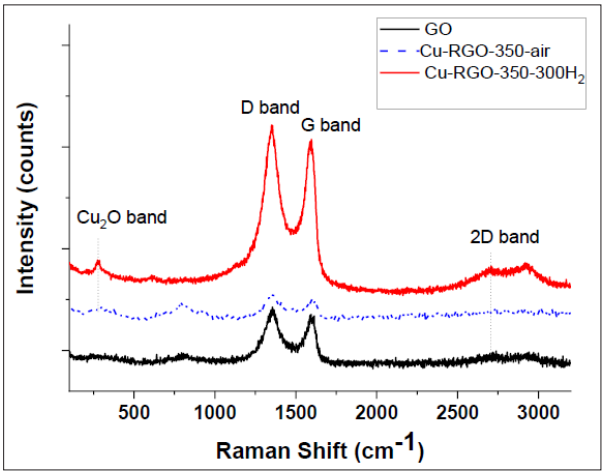


**Figure 3S:** Raman Spectra of GO and Cu-RGO (2:5) nanocomposite heat treated at different temperature and atmospheric conditions, showing G, D and 2D band.

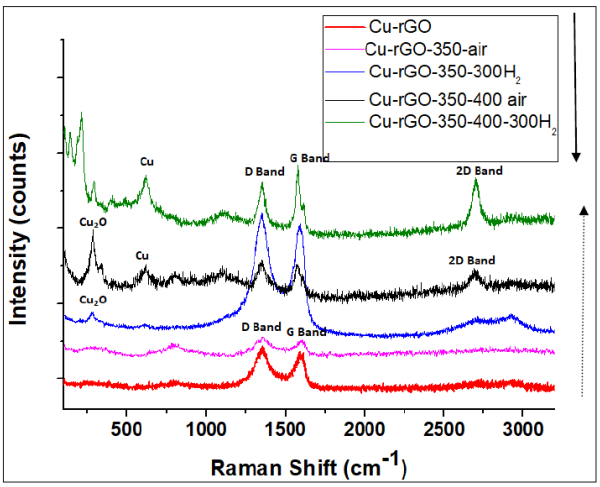


**Figure 4S:** Raman Spectra of Cu-rGO (2:5) or Cu/RGO (2:5) nanocomposite heat treated at different temperature and atmospheric conditions, shown in sequential order (as per indicated by direction markers) to evaluate the stability of the Cu/RGO composite.

## Enhancement factor (EF) calculation

### *Calculation for Cu/RGO (2:5) composite*

To calculate the enhancement factor, the following experimental conditions were used to obtain the Raman Spectra from a Micro Raman Spectra (Renishaw). Laser: 785 nm diode laser, Grating: 1200 $cm^{-1}$, Laser power: 1 mW, objective lens: 20*x*, Numerical Aperture: 0.4. The diameter of the laser spot is taken as 1 µm (calculated from the equation $d = 0.61\lambda/NA$ where $\lambda$ = 785 nm, wavelength of the laser and NA = 0.4) and penetration depth as (*h*) as *x* µm, the focal volume becomes 1.12 x $10^5$ *x* $\mu m^3$ (using the equation $\pi(d/2)2h$).

From ICP-MS, No. of Cu atoms calculated to be present in 0.67g of Cu/RGO = 2.1683 *x* $10^5$. No. of Cu atoms calculated to be present in focal volume = 2.422 *x* $10^5$ *x*.

Considering the molar volume of Cu as 7.11 $cm^3$/mol, volume of one Cu atom is 1.1804 x $10^{-2}$ $nm^3$.

Therefore, the total volume of 2.422 *x* $10^5$ *x* Cu atoms is 2.86 *x* $10^3$ *x* $nm^3$. Taking size of one Cu atom (as 14 nm), volume of one Cu atom = 2744 $nm^3$.

Surface area of one Cu atom is evaluated to be 196 $nm^2$, the total surface area of one Cu atom = 1224.73 *x* $nm^2$.

From the literature, the surface area of 1 MB molecule = 0.8723 $nm^2$, the number of MB molecules adsorbed on Cu nanoparticle is calculated to be Nads = 234.13 *x*.

Considering the density of MB molecules as 1.757 g/ml, the number of MB molecules present in the focal volume (Nbulk) = 0.3705 x $10^{10}$ *x*.

ISERS/IRaman is evaluated using the integrated intensity of MB band at 1618 $cm^{-1}$ from surface enhanced and Raman Spectrum for MB concentration $10^{-4}$ order.

Now,

EF= ( $I_{Sers}$ *x* $N_{Bulk}$ ) / ( $I_{Raman}$ *x* $N_{Abs}$)

We get enhancement factor as 1.28 x $10^8$

In similar way, EF value of the MB solution of concentration $10^{-6}$ and $10^{-8}$ is calculated to be 3.25 x $10^7$ and 1.9 x $10^7$, respectively.

In the above calculations the laser penetration depth (*h*) for SERS substrate and bulk MB powder has been considered same (*x* µm).

**Copyright:** ©2026 Samar Kumar Medda. This is an open-access article distributed under the terms of the Creative Commons Attribution License, which permits unrestricted use, distribution, and reproduction in any medium, provided the original author and source are credited.